RSC Advances

ROYAL SOCIETY OF CHEMISTRY

www.rsc.org/advances

Gold nanoparticles from indole-3-carbinol exhibit cytotoxic, genotoxic and antineoplastic effects through the induction of apoptosis

Ananya Pradhan[1], Madhubanti Bepari[1], Pralay Maity[1], Sib Sankar Roy[2], Sumita Roy[3], Sujata Maiti Choudhury[1*]

[1]Department of Human Physiology with Community Health, Vidyasagar University, Midnapore-Midnapore 721 102, West Bengal, India.E-mail:smaitichoudhury@yahoo.com; Tel: +91 94 7444 4646.

[2]Cell Biology and Physiology Division, Indian Institute of Chemical Biology, Council of Scientific and Industrial Research, 4 Raja S. C. Mullick Road, Kolkata-700 032, India.

[3]Department of Chemistry and Chemical Technology, Vidyasagar University, Midnapore-Midnapore 721 102, West Bengal, India.

Abstract

Synthesis of gold nanoparticles using indole-3-carbinol (AuNPI3Cs) has been extensively studied and presented here. Several techniques have been used to characterize the AuNPI3Cs. Ultraviolet spectroscopy studies indicated the stability of the synthesized AuNPI3Cs, while FTIR analysis proved that indole-3-carbinol was playing an important role in stabilizing the AuNPI3Cs. TEM analysis study showed that AuNPI3Cs were mostly spherical in shape with an average particle size of 3 nm. The selected area electron diffraction pattern exhibited the crystalline nature of AuNPI3Cs, which was further proved by XRD studies. The present study describes the *in vitro* antineoplastic efficacy of AuNPI3Cs against Ehrlich ascites carcinoma (EAC) cells. Results showed that the IC_{50} dose of AuNPI3Cs was significantly capable to elevate intracellular reactive oxygen species. AuNPI3Csinduced apoptosis by increasing the G_2/M population, LIVE/DEAD cytotoxicity, chromatin condensation, DNA laddering and TUNEL-positive cells significantly ($p<0.001$).Reduction ofmitochondrial

potential by AuNPI3Cs was substantiated by JC-1 fluorescent staining. These findings will enlighten the future biomedical application of gold nanoparticles using indole-3-carbinol (AuNPI3Cs) as an antineoplastic agent.

Keywords: Indole-3-carbinol (I3C); Gold nanoparticles (AuNPI3Cs); Ehrlich Ascites Carcinoma (EAC); Intracellular reactive oxygen species; Apoptosis

Introduction

Recent improvement in nanotechnology has designed nanomaterials utilizing nanobased-systems for various biomedical applications. This rapidly developing field of nanotechnology has raised the possibility of using therapeutic nanoparticles in the diagnosis and treatment of different cancers types[1]. Nanoparticles are potential alternatives for treatment of diseases because they have unique biologic effects based on their structure and size, which differ from traditional small-molecular drugs. In the last few years, many pharmaceutical companies have got approval from the US Food and Drug Administration (FDA) for the development of nanotechnology-based drugs. A report based on a study by the European Science Foundation has defined that there is an urge for large investment in developing new nanotechnology based medical tools for therapeutics.[2]

Among the variety of nanoparticles with their applications, metal nanoparticles are playing most important role in biology and medicine [3,4,5]. The synthesis of gold nanoparticles has been extensively studied since the decade of 19th century[6]. The synthesis of gold nanoparticles (AuNP) by reduction of Au ions to Au0 with the use of citric acid has been reported[7]. However, production of gold nanoparticles by the conventional techniques is not eco-friendly due to use of toxic, organic solvents, which greatly limit to its application in biomedical field.

So, green biotechnology ensures non-toxic and eco-friendly methods to synthesize nanoparticles with well-defined shape and size[8]. The green biosynthesis of nanoparticles is gaining more importance over chemical methods. It has promising applications in biomedical fields due to its chemical stability, simplicity, cost effectiveness, easy preparation, optical properties, convenient surface bioconjugation and lower toxicity[9,10,11,12]. Green synthesis involves three distinctive procedural characteristics, using environmentally acceptable solvent system, eco-friendly reducing and capping agents. The use of plant parts or whole

plants or phyto-compound in green synthesis is aninteresting prospect in the reduction of toxicity of nanoparticles in recent years that goes through under enormous investigation.

In the field of green synthesis of metal nanoparticles, the synthesis of gold nanoparticles using living plants[13]was first reportedby Gardea-Torresdey and his co-workers. Synthesis of gold nanoparticles using *Chenopodium album* leaf extract[14] also had been reported.

From environmental issues, it is clear that the green synthesis meets the significant potential in utilization of non-toxic, renewable materials towards nanoparticle synthesis. Many efforts have been directed toward this area with the use of natural products, such as leaf of lemongrass, (*Cymbopogonflexuosus*) [15]and some bacterial species *Thermomonospora* sp.[16], *Rhodopseudomonas capsulate*[17],*Geobacter sulfurreducens*[18], *Bacillus subtilus*[19],*Escherichia coli*[20].

Nowadays, metal nanoparticles exhibit novel chemical and physical properties due to their small size and high surface area which have paid much attention in biomedical field. Currently, metal nanoparticles have drawn tremendous consideration because of their excellent properties on biomedical fields such as in cancer diagnosis and therapy. AuNPs are particularly excellent candidates to improve cancer therapy[21].The therapeutic value of AuNPs is based on their distinguishable physical properties such as enhanced permeability and retention characteristics, excellent surface plasmon resonance and lesser toxicity, increase their ability to interact with cancer cells.

Side effects of several chemotherapeutic drugs have drawn the great attention of many researchers to find out a new class of anticancer agents with more biocompatibility. Although the anticancer activities of several metal nanoparticles have been well studied by many researchers, the main drawbacks of those studies were a lack of selectivity and cytotoxicity towards normal healthy cells. Very little attention has been paid to the studies regarding the anti cancer effect of gold nanoparticles using a phyto-compound, indole-3-carbinol (I3C) on

carcinoma cell till now. Therefore, the present study has been focused on to synthesize and characterize gold nanoparticles (AuNPI3Cs)using indole-3-carbinoland to investigate its cytotoxic, genotoxic and antineoplastic activities against Ehrlich ascites carcinoma (EAC) cell by the induction of apoptosis.

Experimental section

Materials

Indole-3-carbinol was purchased from Sigma Aldrich Co, LLC, US.

Chemicals and culture media

Analytical grade chloroauric acid, RPMI 1640, penicillin and streptomycin were purchased from Sigma Aldrich Co, LLC, US. Fetal bovine serum (FBS), JC-1 was purchased from GIBCO. Dimethyl sulfoxide (DMSO), sodium dodecyl sulphate (SDS), rhodamine 123, propidiumiodide, 3-(4,5-dimethyl-2-thiazolyl)-2,5- diphenyl-tetrazolium bromide (MTT) reagents, standard drug 5-fluorouracil were purchased from Himedia, India. 5,5'-Dithio-bis-(2-nitrobenzoic Acid) (DTNB), Tris–HCl, Tris buffer, Titron X-100, phenol, chloroform, iso-amyl alcohol, ethidium bromide (EtBr) and 2-vinylpyridine were procured from Merck-Millipore (India) Pvt. Ltd. Mumbai. All other chemicals were from Merck Ltd., SRL Pvt. Ltd., Mumbai, and were of analytical grade.

Synthesis of gold nanoparticles using Indole-3-carbinol

Indole-3-carbinol (0.05 mg ml^{-1}) was suspended in triple distilled water. Gold nanoparticles of I3C were synthesized treating an aqueous solution of 0.5 Mm chloroauric acid ($HAucl_4$)

with the solution of indole-3-carbinol at 60˚C with the help of magnetic stirrer[22]. Then, the colloidal solution was left for 24 h at room temperature. The formation of AuNPs of I3C (AuNPI3Cs) was confirmed as observed by the color change of this colloidal solution.The appearance of light violet color confirms the reduction of chloroauric acid into AuNPI3Cs by indole-3-carbinol solution.

Cell line culture and maintenance

Ehrlich Ascites carcinoma (EAC) and DAL (Dalton Ascites Lymphoma) cell lines were obtained from Indian Institute of Technology, Kharagpur, India and Chittaranjan Cancer Research Institute, Kolkata respectively. Male albino (Swiss) mice weighing between 18–25 g were used for the maintenance of these cell lines. The mice were housed in polyacrylic cages (38 x 23 x 10 cm) and were maintained in a constant room temperature of 28–30°C and 55–65% humidity and a controlled day length, 14 hours light and 10hours dark cycle with access to standard pellet diet and drinking water ad libitum. EAC and DAL cell lines were maintained by weekly intraperitoneal transplantation in the abovesaid mice at the concentration of 2 x 10^6/cells/mouse. Washed EAC cells free from contaminating RBC were cultured in RPMI-1640 medium supplemented with 10% fetal bovine serum (FBS), and antibiotic solution (100 U ml^{-1} penicillin, 10 mg ml^{-1}streptomycin and 4 mM L-glutamine) under 5% CO_2 and 95% humidified atmosphere at 37˚C in a CO_2 incubator[23]. $1\times10^6 ml^{-1}$ viable cells were used for different experiments in the present study. The study was approved by the Institutional Animal Ethical Committee (IAEC), registered under Committee for the Purpose of Control and Supervision of Experiments on Animals (CPCSEA), Ministry of Environment, Forests & Climate Change, Govt. of India and performed in compliance with the relevant laws and guidelines of the CPCSEA.

Isolation of mice lymphocyte cell (MLC):

Blood samples were collected from healthy above mentioned male mice by 5 ml heparin-coated Vacutainers according to the method of Hudson and Hay[24]. About 3 ml of blood were layered onto same amount of Histopaque 1077 (Sigma-Aldrich Co. LLC, US) and centrifuged at 2000 rpm for 30 min at room temperature. The upper monolayer of buffy coatcontaining lymphocytes was transferred to a clean centrifuge tube and washed three times in balanced salt solution (PBS). The mice lymphocytes (MLCs) were re-suspended in RPMI complete media supplemented with 10% FBS and incubated for 24 h at 37˚C in a 95% humidified and 5% CO_2 atmosphere in a CO_2 incubator.

Drug preparation from AuNPI3C

AuNPI3Cs (1mg/ml stock) was prepared by concentrating the solution with RPMI media. The solution of AuNPI3Cs was then sonicated and was used for the assessment of biopharmacological activities.

Experimental Design

EAC (1×10^6 cells) cells were exposed to different concentrations (1, 5, 10,25 and 50µg ml^{-1}) of AuNPI3Cs for 24 h. Control EAC cells did not receive AuNPI3Cs exposure; it was only maintained with a required amount of complete culture media. After the treatment schedule, the cells were collected separately from the petri plates and centrifuged at 1000-1200 rpm for5 min at 4°C to separate cells and supernatants. The cells were washed twice with 0.1 MPBS (pH 7.4). A required amount of cells was lysed using hypotonic lysis buffer for 45 min at 37ºC and then processed for biochemical estimations. Intact cells were used for

mitochondrial membrane potential, ROS measurement, TUNEL assay and different microscopic observations.

A. Characterization of AuNPI3Cs

Dynamic light scattering(DLS) study and measurement of surface zeta potential

Dynamic light scattering considered as photon correlation spectroscopy is a non-invasive technique for measuring the size of particles. Particle size measurement was analysed using Stokes-Einstein relationship.

The formula is $rk = \frac{kT}{6\pi nD}$ (1),

Where as k is the Boltzmann's constant, T the temperature in k; n the solvent viscocity; D is the diffusion coefficient.The freshly prepared AuNPI3Cs were used for particle size and zeta potential measurements. Hydrodynamic diameters were measured by DLS[25]; Zetasizer Nano ZS; Malvern Instruments, (Malvern,UK). The polydispersity index (PDI) was assessed that representing the distribution of particle size. DLS measurements were performed at 25˚C. The surface charge was expressed by zeta potential. The pH value of AuNPI3Cs was fixed in both experiments.

Ultraviolet spectroscopic (UV-Vis) study

UV-vis spectroscopy was utilized to quantitatively characterize nanoparticles. A sample is used to expose with electromagnetic waves in the ultraviolet and visible ranges. Analysis of the absorbed light was performed through the resulting sprectrum. Synthesis of AuNPI3Cs by the reduction of chloroauric acid using indole-3-carbinol was easily observed by UV-Vis spectroscopy[26]. UV-visspectroscopy of AuNPI3Cs was carried out on a UV-vis Spectrophotometer (UV-245 Shimadzu, Japan).

X-ray diffraction (XRD) study

Nowadays, X-ray diffraction is extensively used technique for the characterization of nano particles. The interaction of X-ray radiation with crystalline sample is predicted by Bragg's law. The quantitative account of Bragg's law can be expressed as:

$2d_{hkl} \sin \theta = n\lambda$ (2),

where d is the interplanar spacing for a given set of hkland θ, the Bragg angle. The powder XRD measurements were carried out using a X-ray diffractometer (PHILIPS 1710). To determine the crystallinity of AuNPI3Cs an operating voltage was set to 30 kV at wavelength 0.154 nm (Cu-Kα)and the operating current was adjusted to 40 mA and 2θ = 20°–70° [27]. The phase identification for AuNPI3Cs reported in this study was performed by matching the peak positions of XRD patterns with the patterns of the JCPDS (Joint Committee on Powder Diffraction Standards) database.

Fourier transform infrared spectroscopy of AuNPI3Cs

The formulation of gold nanoparticle with indole-3-carbinol was investigated by Fourier transform infrared (FTIR) spectroscopy with a Perkin Elmer Spectrum FTIR systemusing a (Perkin Elmer Spectrum Express Version 1.03.00)[28].The powdered sample was mixed with KBr preparing the pellets and FTIR spectra were observed. The instrument wavelength ranges from 4000 to 400cm^{-1} with an accuracy of ±0.01cm^{-1} and resolution of 4cm^{-1}. The spectrum of the sample was measured after setting the reference spectrum of KBr pellet for accuracy.

High resolution transmission electron microscopic (HR-TEM) study

TEM is a microscopic technique where emitted electrons from an electron source are focused into a very thin beam which are transmitted through the sample and finally projected on a

fluorescent screen giving a shadow image of the sample. The particle size and microstructure of AuNPI3Cs were studied by CM12 PHILIPS high-resolution transmission electron microscope operating at 200 kV[29]. Briefly, synthesized AuNPI3Cs were sonicated using a sonicator bath until it formed a homogeneous suspension. Then a drop of homogenous AuNPI3Cs suspension was given onto a carbon-coated copper grid and was dried in air and placed it under transmission electron microscope and fitted with a CCD camera and was observed.

Scanning electron microscopic (SEM) study

Scanning electron microscopy (SEM) can provide a highly magnified image of the surface and the information regarding the composition of near surface regions of nano particles. Scanning electron microscope (SEM), (CAMSCAN-2 JEOL, Japan) was used to determine the shape of AuNPI3Cs. Samples were prepared by depositing a drop of solution on a glass slide (1×1mm) and drying at vacuum desiccator. Samples were placed in sample stub using adhesive carbon tape and then the samples were gold coated with the help of JEOL auto fine coater-JEOL1600 and were placed under the microscope for observation[29].

Energy dispersive X-ray analysis (EDX)

Energy dispersive X-ray analysis is a technique to analyse elements composition and estimate their proportions[30]. EDX (OXFORD) study was used to confirm the presence of gold particles as well as to detect the other elemental compositions of the synthesized AuNPI3Cs. The EDX spectrum was obtained at an acceleration voltage of 20 kV and was collected for 19s.

B. Cytotoxicity study by MTT assay

***In vitro* cell viability assay (MTT assay)**

MLC, EAC and DAL cells were maintained in RPMI-1640 supplemented with 10% FBS, penicillin (100 U ml^{-1}), and streptomycin (10 mg ml^{-1}) in a humidified atmosphere of 5% CO_2at 37˚C. The cytotoxicity of synthesized AuNPI3Cs on MLC, EAC and DAL cells was determined by the MTT assay. Cells (1×10^6 per well) were plated in 100 µl of medium per well in 96 well plates and then the cells were incubated after the treatment of I3C and AuNPI3Cs for 24 h at 37˚C. After removal of the treated compound and washing with PBS (pH 7.4), 5 mg ml^{-1} of 0.5% MTT in phosphate-buffered saline solution were added in each well. After 3 h of incubation, 0.1% DMSO was added to each well. Viable cells were measured at the absorbance of 540 nm[31]. The optical density (OD) at 540 nm was measured on ELISA ANALYSER (Bio-Rad, Model 680). All experiments were performed in triplicate, and the effect of AuNPI3Cs on the proliferation of EAC and DAL cells was expressed as the % of cell viability using the following formula:

$$\% \text{ cell viability} = [OD_{sample} - OD_{control}] \times 100/OD_{control} \quad (3)$$

C. Study on Oxidative stress

Estimation of reduced glutathione (GSH)

At first each sample (0.2 ml) was mixed with 4% sulfosalicylic acid and centrifuged at 2000 rpm for 10 min to settle the precipitated proteins. In aspirated supernatant 2 ml of 0.6 mM DTNB was added. Then the optical density of the yellow-colored complex formed by the reaction of GSH and DTNB was measured at 412-420 nm[32]. GSH contents were expressed as µg of GSH mg^{-1} protein.

Determination of oxidized glutathione (GSSG)

The oxidized glutathione level was measured after derivatization of GSH with 2-vinylpyridine. In brief, with a 0.1 ml sample, 2 µl of 2-vinylpyidine was added and incubated for 1 h at 37°C. The mixture was then mixed with 4% sulfosalicylic acid and centrifuged at 3000 rpm for 10 min to settle the precipitated proteins. The supernatant was aspirated and the GSSG level was estimated with the reaction of DTNB at 412 nm[33]. The levels of GSSG were expressed as µg of GSSG mg^{-1} protein.

Intracellular ROS measurement

Intracellular ROS measurement was performed using 2′, 7′-dichlorodihydro fluorescein diacetate (H_2DCFDA)[34]. EAC cell lines were treated with AuNPI3Cs at 5 µg $ml^{-1}$for 24 h. After treatment, cells were washed with phosphate buffer followed by incubation with 1 µg ml^{-1} H_2DCFDA for 30 min at 37 ºC. The cells were again washed three times with fresh culture media. DCF fluorescence was determined at 485 nm excitation and 520 nm emission using a Hitachi F-7000 Fluorescence Spectrophotometer and was also observed by fluorescence microscopy (LEICA DFC295, Germany). All measurements were done in triplicate.

Protein Estimation

EAC cell protein was estimated according to the method of Lowry *et al*, (1951)[35] using BSA (Sigma,Aldrich) as a standard.

D. Induction of apoptosis

Chromatin condensation by DAPI and propidium iodide staining

Changes during the initial phase of apoptosis are associated with chromatin condensation around the nuclear membrane. These nuclear changes were observed in EAC cells by 4′,6′-Diamidino-2-phenylindoledihydrochloride (DAPI) and propidium iodide (PI), staining. The nuclear changes in the apoptotic cells were observed by DAPI and PI staining was performed according to Prasad and Koch,2014[36] with few modifications. EAC cells (1×10^6cells ml^{-1}) were seeded in petriplate and incubated with 5 μg $ml^{-1}$of AuNPI3Cs for 24h at 37°C and 5% CO_2. The cells were then fixed by 70% ethanol incubation at −20°C for 2 hours. After fixation, cells were washed and stained with DAPI (1 μg ml^{-1}) at 37°C for 5 minutes and RNAse-propidium iodide (PI) mixture (1mg ml^{-1}) at 37°C for 15 minutes. The cells were washed with phosphate buffer and observed under fluorescence microscope (LEICA DFC295, Germany).

Cellular morphology analysis by acridine orange–ethidium bromide double staining

Cellular morphology analysis by acridine orange (AO) and ethidium bromide (EtBr) double staining is the probable pathway of cell death. Here the cells were analyzed by the AO-Etbr double staining method[37]. A number of 1×10^6 EAC cells were seeded into each well of plate and incubated for 24 h at 37˚C in a humidified 5% CO2 atmosphere. AuNPI3Cs at 5 μg ml^{-1}were then added to the well for 24 h. After incubation, cells were washed with PBS buffer. Then on a clean glass slide 10 μl of washed cells were placed and 10 μl each of acridine orange (50 μg ml^{-1}) and ethidium bromide (50 μg ml^{-1}) were mixed. Then cells were observed under a fluorescence microscope (LEICA DFC295, Germany).

DNA fragmentation study by agarosegel electrophoresis

At first, 1×10^6 ml^{-1} EAC cells were subcultured in the culture medium and incubated for 24 h at 37˚C in a humidified 5% CO_2 atmosphere and AuNPI3Cs at 5 μg$ml^{-1}$and standard drug 5-

FU were then added to culture medium for 24 h. After 24 hr cells from treated groups were centrifuged at 1000-1200 rpm to obtain the pellet containing both intact and apoptotic cells. Cells were further washed with phosphate buffer saline, (pH 7.4) and again centrifuged at 1200-1500 rpm. Before overnight lysis of the cell pellet 150-200 µL of lysis buffer (10 mM EDTA, 0.5% SDS, 10 mM Tris base and 0.5 µg ml^{-1} Proteinase K; pH 7.5) was mixed. After 16 h, RNAse (0.5 µg ml^{-1}) solution was added to it and incubated at 37 °C for 2 h. DNA was then isolated by phenol–chloroform-isoamyl alcohol extraction method[38]by vortexing the lysate 10 times min^{-1} cycle. DNA in the aqueous phase was collected and precipitated by 7.5 M ammonium acetate and ice cold dehydrated ethanol, then incubated overnight at -20^0C and DNA was dissolved in 20 µl TE buffer (pH 7.4). The total 20 µl DNA solution on DNA electrophoresis was performed in 1.5% agarose gel containing 1 µg ml^{-1}ethidium bromide at 75 volt, and DNA fragments were visualized by exposing the gel to UV light and image was captured by Gel-doc (Bio-Rad) apparatus.

Terminal deoxynucleotidyl transferase-mediated dUTP nick end labeling (TUNEL) assay

Apoptosis was also examined by using the TUNEL assay to detect DNA strand breaks during apoptosis using an *In Situ* Cell Death Detection Kit,Fluorescein,Version:17(Cat No: 11684795910) according to the manufacturer's instructions[39]. Briefly, EAC cells were treated with AuNPI3Cs (5µg/ml) for 24 hrs and fixed with freshly prepared 3.7% paraformaldehyde in phosphate-buffered saline (PBS; pH 7.4) for 30 min. The EACcells were then suspended with 100µl permeabilization solution (0.1% Triton X-100 in 0.1% sodium citrate buffer) for 2 min in ice-chilled condition [$(2\text{-}8)^0$C temperature]. The suspended cells were washed three times with PBS buffer and incubated with 50µl TUNEL reaction mixture for 60 min at

37˚C.The stained cells were analysed using flow cytometer (BD FACSVerse) an excitation wavelength in the range of 488 nm and detection in the range of 515–565 nm.

Measurement of Mitochondrial membrane potential (ΔΨm) by Rhodamine 123

The alteration of mitochondrial membrane potential was measured by the spectro-fluorometric method[40]with some modifications. In brief, EAC cell lines were treated with AuNPI3Cs at 5 μg ml^{-1} for 24 h. After treatment, cells were washed with culture media followed by incubation with 1.5 μM Rhodamine 123 for 15 min at 37ºC in a humidified chamber. The cells were then washed three times with culture media. The fluorescence intensity of Rhodamine 123 was monitored for 2 min using a Hitachi F-7000 Fluorescence Spectrophotometer. An aliquot of cell suspension was also used for microscopic observations (LEICA DFC295, Germany). The cellular mitochondrial membrane potential was expressed as a percentage of control cells at an excitation wavelength of 493 nm and an emission wavelength of 522 nm. Both the excitation and emission slit width were set to 5.0 mm.

Study of Mitochondrial membrane potential (ΔΨm) by JC-1

Intensity of mitochondrial membrane potential of intact cells was measured by spectrofluorometrically[41] with the lipophilic cationic probe 5,5 V,6,6 V-tetrachloro-1,1 V 3,3 V-tetra ethylbenzimidazolcarbocyanine iodide (JC-1),which explores potential-dependent fluorescence in mitochondria. At low membrane potentials in mitochondria, JC-1 produces a green fluorescence (emission at 527 nm). At high membrane potentials, JC-1 produces a red fluorescence(emission at 590 nm). Briefly, EAC cells were treated with AuNPI3Cs at 5 μg ml^{-1} for 24 h for the assay, and after discarding the culture medium, staining solutions (0.5 ml) with JC-1 dye was added to the cells. Cells were then incubated at 37°C for 15 min in a CO_2 incubator and, after discarding the medium, washed twice with 1 ml of assay buffer and

the cell suspension was measured by using a Hitachi F-7000 Fluorescence Spectrophotometer. An aliquot of cell suspension was used for microscopic observations (LEICA DFC295, Germany).

DNA fragmentation study by alkaline comet assay

DNA fragmentation was further assessed by alkaline comet assay with few modifications[42].Briefly, EAC cell lines were treated with AuNPI3Cs at 5 μg $ml^{-1}$for 24 h. After treatment, cells were washed with phosphate buffer. Then the cell pellet was mixed with 0.7% agarose for performing the comet assay. The glass slide was smeared with 1% agarose and covered with cell pellet. After that slides were poured in lysis buffer and electrophorized. Then the slides were stained with fluorescence stain ethidium bromide and image was captured under fluorescence microscope (LEICA DFC295, Germany).The comet tail length was calculated as the distance between the end of heads and end of each tail. Tail moments were defined as the product of the percentage of DNA in each tail,[43]and % DNA (tail) presented as: TA × TAI × 100/ [(TA × TAI) +(HA × HAI)]; where as TA= tail area, TAI = tail area intensity, HA= head area and HAI = head area intensity. All measurements were done in triplicate.

Detection of cellular apoptosis by flow cytometry

Cell cycle study was measured by flow cytometric analysis[44]. Briefly, after AuNPI3Cs exposure (5 μg ml^{-1}) for 24 h the cells were centrifuged at 2000 rpm for 5 min. After washing, cells were resuspended in PBS. Cells were incubated with RNase (10 mg ml^{-1}) solution for 1 hr at 37˚C. After incubation cells were stained with propidium iodide (1mg ml^{-1}) (Sigma, Aldrich) for 15 min at room temperature at dark. Then cells were washed with

PBS buffer and diluted with 500 µl PBS. Then, the cell cycle was analyzed using flow cytometer (BD FACSVerse) and Cell Quest software.

Statistical analysis

All the parameters were assayed in triplicate manner. The data was expressed as mean ± SEM, Comparisons between control and treated groups were analysed by using the one-way ANOVA test (using a statistical package, Origin 6.1, Northampton, MA), $p<0.05$ as a limit of significance.

Results and discussion

Average size analysis from Dynamic light scattering (DLS) study

From dynamic light scattering (DLS) the mean size of AuNPI3Cs particles (in aqueous solution) was measured. The average size (z-average) of nanoparticles from DLS measurements (Fig. 1) was 7nm. The zeta-potential measurement showed that AuNPI3Cs had a negative zeta potential of -18.8mv and this negative surface charge may be due to the aggregation of more gold metals on the surface of nanoparticles[45].

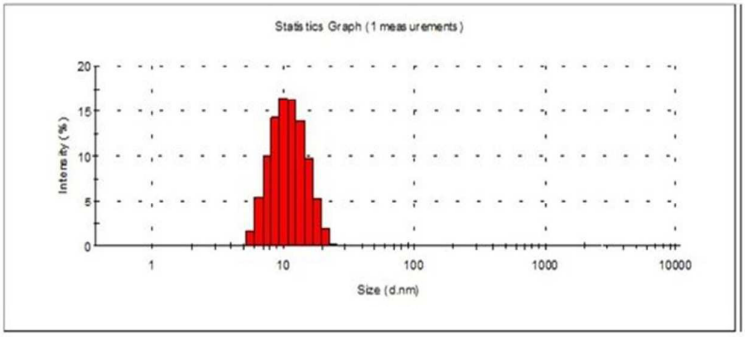

Fig. 1 DLS showing particle size distribution of gold nanoparticles prepared by treating 0.5mM aqueous chloroauric acid solution with indole-3-carbinol (AuNPI3Cs) at room temperature.

UV-Vis absorption spectroscopic analysis

It is reported that gold nanoparticles exhibit a violet colour in aqueous solution due to the excitation of surface plasmon oscillation induced by the electromagnetic field. When Indole-3-carbinol was mixed into an aqueous solution of chloroauric acid, the solution started to change from colorless to light violet color due to the reduction of gold ions. UV-Vis spectroscopy study confirmed that I3C reduce the precursor solution ($HAuCl_4$) to form uniform spherical morphology with high stability gold nanoparticles with the size of 3-7 nm which could be identified from the peaks obtained around 500 nm (Fig. 2). The peak originates from the excitation of electrons of AuNPI3Cs induced by the electromagnetic field[46].

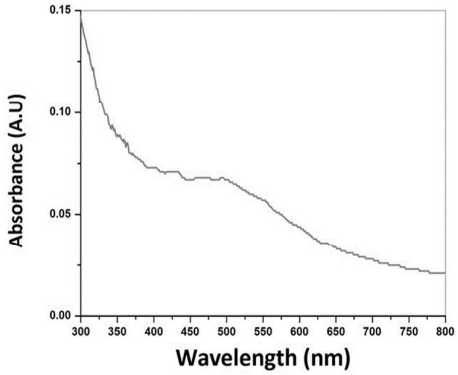

Fig. 2 UV-Vis absorption spectra of AuNPI3Cs at room temperature

X-ray diffraction (XRD) measurement

Fig. 3 shows the XRD patterns of air-dried AuNPI3Cs synthesized. A number of Bragg reflections can be seen with 2θ values of 31.78˚, 38.08˚, 44.63˚, 64.11˚,77.2˚ corresponding to the lattice planes, which may be indexed to (100), (111), (200), (220) and (311) facets of gold, respectively. The XRD pattern showed that the powder sample produced well-defined diffraction patterns (Fig. 3), indicating that they were crystalline in nature, and the peaks matched well with the standard JCPDS cards of the respective metal[47].

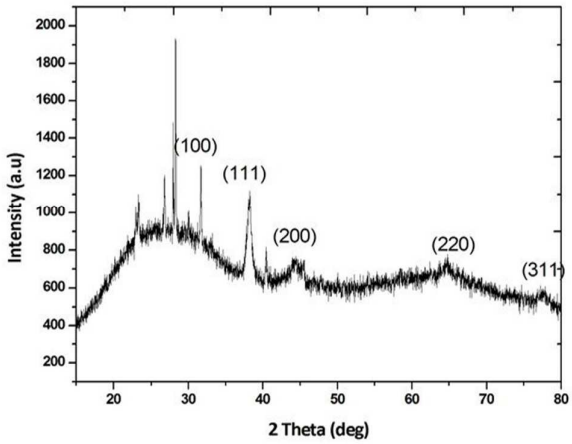

Fig. 3 XRD patterns showing peaks corresponding to the diffraction from (100), (111), (200), (220) and (311) planes of fcc lattice of AuNPI3Cs.

FTIR Analysis

The FTIR spectra of indole-3-carbinol and synthesized AuNPI3Cs are shown in Fig. S1A and S1B.The peak at 3382.98 cm^{-1}[48] belongs to the N–H stretching vibrations of the peptide linkages. The peak at 2870.62 cm^{-1}[49] corresponds to symmetric and antisymmetric vibration bands of CH_2 and CH_3 groups of amino acid side chains. The peak at 1663.52 cm^{-1} [50]belongs to mainly the stretching C=O and bending. The peak at 1454.22 cm^{-1} [51]indicates to bending CH_2 modes. The FTIR spectrum for AuNPI3Cs is represented in Fig. S1B. The shifts in the peak positions from 3382.98, 2870.62, 1663.52, 1454.22, and cm^{-1} to 3405.74, 2835.35, 1694.88, and 1457.73 cm^{-1}, respectively, of the synthesized AuNPI3Cs indicates that indole-3-carbinol are involved in reducing and stabilizing the gold nanoparticles.

Transmission electron microscopy (TEM) measurement

High-resolution transmission electron microscopic (HRTEM) study was used for morphological analysis of synthesized AuNPI3Cs. From Fig. 4 it is clear that the synthesized AuNPI3Cs are mostly spherical in nature. TEM analysis (Fig. 4) showed that formation of gold nanoparticles was done with spherical and circular shape and had sizes of 2-4 nm. A small difference was observed in the diameter range obtained from TEM and DLS measurement. The particle size determined by TEM represents the actual diameter of the nanoparticles as the TEM study was done in the dry state of the sample, whereas the size measured by light scattering method is a larger hydrodynamic diameter due to the hydrated state of the sample[52].The crystallinity of the AuNPI3Cs was further recognized by the selected area electron diffraction (SAED) pattern with bright circular spots (Fig. S2).

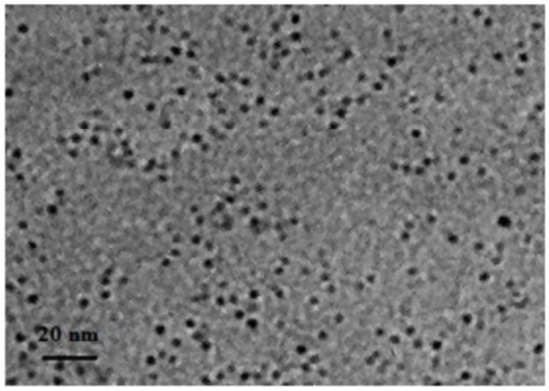

Fig. 4 HRTEM images of gold nanoparticles treating 0.5mM aqueous chloroauric acid solution with indole-3-carbinol.

Scanning electron microscopy (SEM) measurement

Scanning electron microscopy was used to analyze the morphology and size of the synthesized goldnanoparticles. From SEM images (Fig. S3) it was clear that the nanoparticles were mostly spherical with a distribution of uniform shape.

Energy dispersive X-ray analysis

The elemental composition analysis by energy dispersive X-ray (EDX) indicates the presence of gold particles. The result shows a strong absorption peak at 2 keV, which is mainly for the absorption of metallic gold nanoparticles and other peaks are shown at 8-14 keV (Fig. 5).

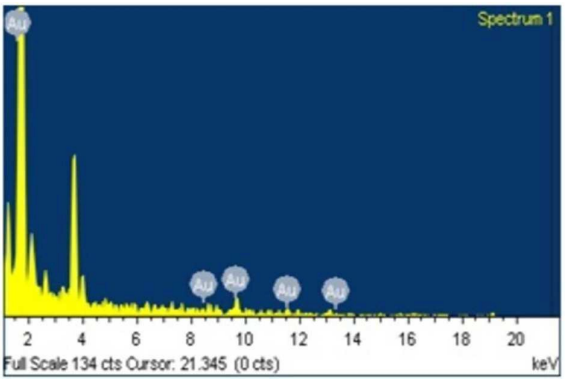

Fig. 5 shows the energy dispersive spectrum of gold nanoparticles treating 0.5mM aqueous chloroauric acid solution with indole-3-carbinol.

***In vitro* cell proliferation assay**

EAC cells were exposed to I3C and AuNPI3Cs at various concentrations for 24 h, and cytotoxicity was determined using the MTT assay (Fig. 6 & 7). The reduction in viability of AuNPI3Cs treated cancer cells occurs in a dose-dependent manner. The AuNPI3C significantly decreased EAC cell viability by 35.24%, 51%, 61.08% ,70.15% and 79.77% at 1, 5, 10, 25 and 50 μg ml^{-1} doses respectively. On the other hand, no significant reduction of lymphocyte viability was noted at the doses of AuNPI3Cs up to 50 μg ml^{-1}. From the above result, it is clear that AuNPI3Cs show maximum antiproliferative effect on EAC cells. Mitochondrial assembly might be disturbed by AuNPI3Cs which resulted in the increased cytotoxicity of EAC cells[53].The IC_{50} value of AuNPI3Cs against EAC cells and DAL cells is 5μg $ml^{-1}$and 10μg ml^{-1} respectively whereas IC_{50}value of I3C is 25μg/ml against EAC cell. AuNPI3Cs show DAL cells viability significantly decreased by 27.57% , 37.51%, 50% , 66.4% and 70.12% at 1, 5, 10 , 25 and 50 μg ml^{-1} doses,(Fig. S4) respectively. Finally at the concentration of AuNPI3Cs (5μg/ml) further experiments were performed using this concentration to see the effect of AuNPI3Cs against EAC cell *in vitro* because at this concentration AuNPI3Cs did not show any lethality towards normal cells.

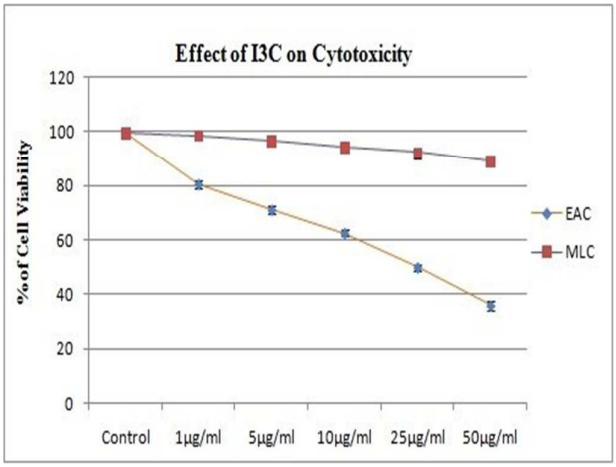

Fig. 6 *In vitro* cell viability assay of EAC cells and mice lymphocyte cells (MLCs) with I3C. Cells were treated with I3C for 24 h at 37°C. Values are expressed as the means ± SEM of three experiments.

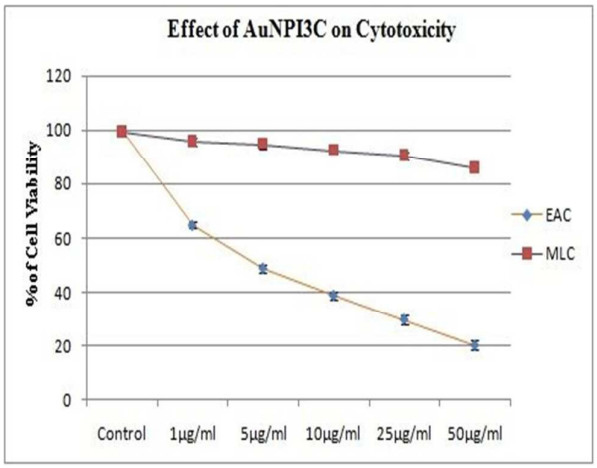

Fig. 7 *In vitro* cell viability assay of EAC cells and mice lymphocyte cells (MLCs) with AuNPI3Cs. Cells were treated with AuNPI3Cs for 24 h at 37°C. Values are expressed as the means ± SEM of three experiments.

Intracellular glutathione level

Reduced glutathione is an important intracellular reductant and offers protections against free radicals and toxic agents. In different pathological conditions and diseases cellular GSH concentrations is depleted by oxidation of GSH to glutathione disulfide (GSSG). This conversion of GSH to GSSG is caused by oxidative stress[54]. In this study it is clear that AuNPI3Cs killed EAC cells by altering the intracellular redox status. The present study showed that GSH level (Fig. S5A) of EAC cells decreased significantly ($p<0.05$) whereas GSSG level (Fig. S5B) increased significantly ($p<0.01$) after the treatment of AuNPI3Cs. Decreased levels of GSH and enhanced levels of GSSG might be as a result of the effective conversion of GSH to GSSG by increased free radicals induced by AuNPI3Cs in EAC cells.

Cellular reactive oxygen species (ROS) level

EAC cells exposed to AuNPI3Cs for 24 h showed increased reactive oxygen species (ROS) formation as evidenced by the increase in fluorescence intensity of the DCF. The results indicate that a significant ($p <0.001$) increase of ROS level is found due to AuNPI3Cs exposure (Fig. 9). The fluorescence images (Fig. 8) are highly correlated with the fluorescence intensity level. ROS are such natural by-product which contains unpaired valence electrons, being highly active and have a specific role in cell signalling and homeostatis[55], leading to oxidative damage. Intracellular ROS generation mainly caused by mitochondrial respiratory chain reaction and membrane-bound superoxide-generating enzyme i.e., nicotinamide adenine dinucleotide phosphate (NADPH) oxidase mediated reactions[56]. In this study, AuNPI3Cs may interrupt mitochondrial membrane integrity of EAC cell, evidenced by MTT assay. The impairment of mitochondrial electron transport chains may elevate ROS generation[57]. Again elevated levels of ROS may stimulate the release of

different pro-inflammatory markers such as TNF-α. TNF-a activates nuclear factor-kB and last of all leads to cell death by apoptotic and necrotic pathways[58].

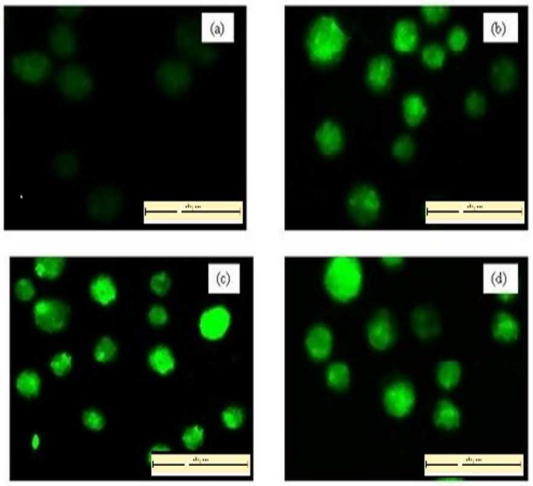

Fig. 8 Fluorescence microscopy of reactive oxygen species (ROS) formation using H_2DCFDA stain. Here, (a) Control; (b) I3C-treated EAC cells; (c) AuNPI3Cs-treated EAC cells; and (d) 5-FU-treated EAC cells. Experiments were repeated in triplicate.

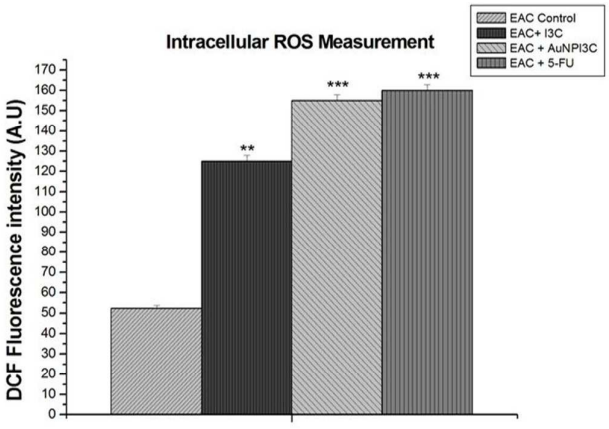

Fig. 9 Effects of I3C, AuNPI3Cs and 5-FU on reactive oxygen species (ROS) induction in EAC cell. DCF fluorescence intensity is indicated by ROS production. Values are expressed as the means ± SEM of three experiments; ** $p<0.01$, *** $p<0.001$, statistically significant difference compared with the control group.

Chromatin condensation

Propidium iodide (PI) and 4′,6′-diamidino-2-phenylindole dihydrochloride (DAPI) staining in apoptosis study were used to visualise condensed chromatin of apoptotic dead cells. The uptake of this dye allows the identification of dead cells. PI stains fragmented nuclear chromatin of apoptotic cells which appears red color whereas the stain is excluded by live cells. Chromatin condensation is a common characteristic of early phase of apoptosis[59]. Fluorescence image of EAC cells stained by PI and DAPI confirmed that AuNPI3Cs have the ability to inhibit the cell proliferation via apoptosis. Treatment of AuNPI3Cs exhibited typical apoptotic morphology (Fig. 10 and Fig. 11) with condensed nuclei in AuNPI3Cs-treated EAC cell compared to EAC control. This can be seen in the appearance of crescents around the periphery of the nucleus or bright blue spherical beads were present on the entire chromatin. As membrane integrity became compromised and PI and DAPI stain leaked into intact membrane, even in shrunken cell, the apoptotic nuclei appeared bright pink chromatin and bright blue chromatin that are highly condensed and fragmented[60].

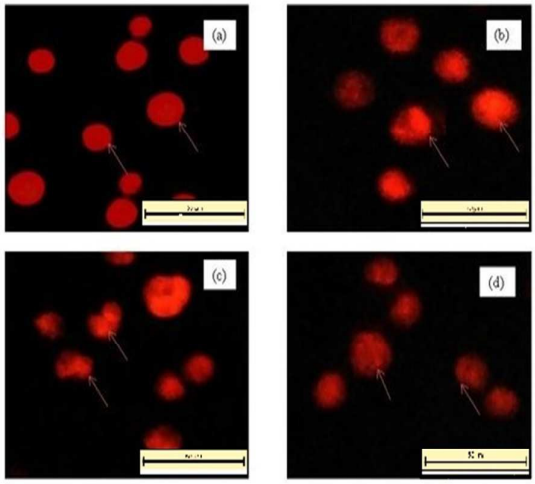

Fig. 10 Chromatin Condensation study in EAC cells. Cells were stained with PI and visualized under a fluorescence microscope. Here, (a) Control; (b) I3C-treated EAC cells; (c) AuNPI3Cs-treated EAC cells; and (d) 5-FU-treated EAC cells.

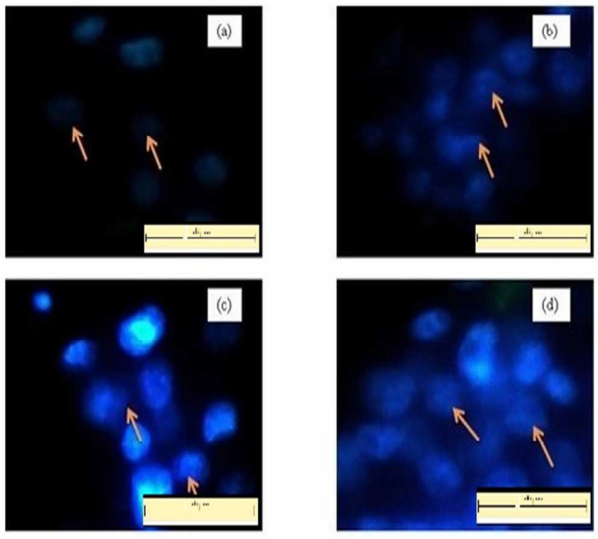

Fig. 11 Chromatin Condensation study by DAPI. Cells were stained with DAPI and visualized under a fluorescence microscope. (a) Control; (b) I3C-treated EAC cells; (c) AuNPI3Cs-treated EAC cells; and (d) 5-FU-treated EAC cells.

EtBr-AO double staining cell morphological analysis

The results obtained from the EtBr-AO double staining are shown in Fig. 12. This staining reveals that the viable cells with intact DNA, having a round and green nucleus. Early apoptotic cells have fragmented DNA, which appears as several green-colored nuclei. Late apoptotic and necrotic cell DNA is fragmented and having orange and red nucleus. From Fig. 12c, it is clear that AuNPI3Cs are able to decrease the number of viable cells tremendously compared to EAC control. Most of the cells exhibit typical characteristics of apoptotic cells.

A very small number of cells are stained red[61]. These results indicate that EAC cell death occurs primarily through the induction of apoptosis by AuNPI3Cs.

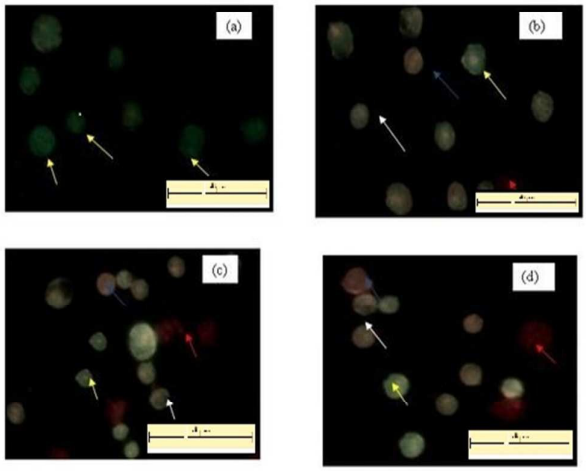

Fig. 12 EtBr-AO double staining study in EAC cells treated with AuNPI3Cs. Cells were treated with EtBr-AO and visualized under fluorescence microscope. Here, (a) Control; (b) I3C-treated EAC cells; (c) AuNPI3Cs-treated EAC cells; and (d) 5-FU-treated EAC cells, Yellow arrow indicates viable cell, white arrow indicates early apoptotic cell, blue arrow indicates late apoptotic cell and red arrow indicates necrotic cell.

DNA fragmentation

DNA damage can result from the action of endogenous ROS in replication, as well as from environmental toxicants. DNA laddering is a valuable technique to analyse the endonuclease cleavage products of apoptosis. ROS can act as signal molecules promoting cell-cycle progression, and induce oxidative DNA damage. DNA fragmentation is broadly considered a

characteristic feature of apoptosis. Induction of apoptosis can be confirmed by two reasons: in which the cells are reduced and condensed, and DNA fragmentation[62]. To confirm the apoptotic features induced by AuNPI3Cs treated EAC cells, a DNA-fragmentation assay was conducted. Fig. S6 clearly indicates that the DNA-laddering pattern in EAC cells treated with AuNPI3Cs is one of the reasons for EAC cell death.

TUNEL assay by *Insitu* cell death detection kit

DNA content of the cells was estimated by TdT mediated dUTP nick end labeling (TUNEL) assay using Flow cytometry (Fig. 13). As shown in Fig. 14 we observed that treatment of EAC cells with I3C, AuNPI3Cs and 5-FU resulted in 4.95%, 17.31% and 13.01% TUNEL positive respectively. The ability of AuNPI3Cs to induce apoptosis is also supported by measuring the DNA damage in cells. As shown in Fig. 13, TUNEL-positive cells were detected by flow cytometry which indicates apoptotic cells with the presence of DNAfragments. During apoptosis, DNA strand breaks expose the 3′OH ends which act as sites for the addition of fluorescein-dUTP[63]. The incorporation was detected using fluorescein-dUTP to label DNA strand breaks[64].

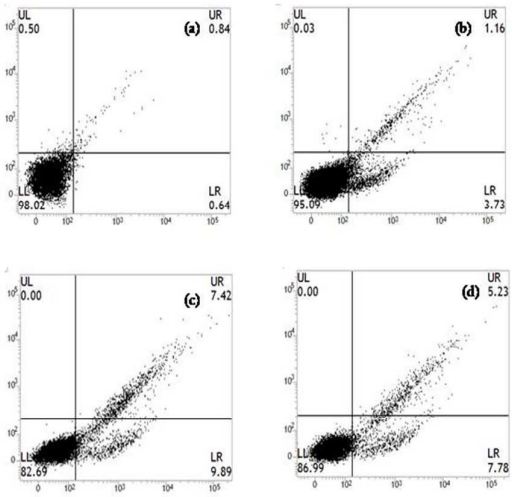

Fig. 13 AuNPI3Cs- induced apoptosis as measured by TUNEL assay. DNA strand breaks were analyzed by flow cytometry. Here, (a) Control; (b) I3C-treated EAC cells; (c) AuNPI3Cs-treated EAC cells; and (d) 5-FU-treated EAC cells.

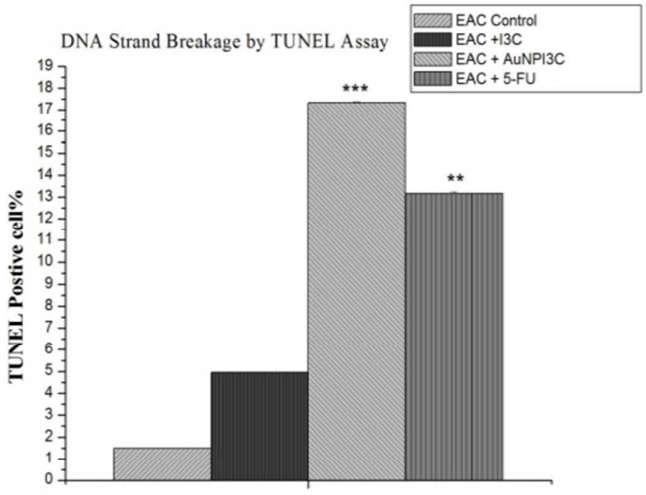

Fig. 14 Analysis of TUNEL positive cell percentage. Apoptotic cells are quantified by counting the percentages of TUNEL-positive nuclei containing cells. Data are presented as means ± SEM of three independent experiments. ** $p<0.01$, *** $p<0.001$, statistically significant difference compared with the control group.

Alteration of mitochondrial membrane potential (MMP, $\Delta\psi_m$)

Determination of mitochondrial membrane potential is based on Rhodamine 123 fluorescence intensity. The percentage of MMP decreased significantly ($p<0.01$) (Fig. S7B) in AuNPI3Cs treated EAC cells. Depletion of mitochondrial membrane potential is another marker of apoptosis-induced cell death[65]. The present study showed that an effective dose (5μg ml^{-1}) of AuNPI3Cs mitochondrial membrane potential was decreased in EAC cell as compared to the control. The strong dissipation in MMP (Fig. S7A) in the cancer cell suggested a possible disruption of the cellular mitochondrial membrane after AuNPI3Cs treatment. Alteration of mitochondrial membrane potential in AuNPI3Cs treated carcinoma cells may result in malfunction in ATP synthesis and maintenance of the ATP level that leads to either apoptosis or necrosis. Apoptosis does not depend only on depleted ATP synthesis, whereas a decreased level of ATP ensures apoptosis induction[66].

Measurement of Mitochondrial membrane potential ($\Delta\psi_m$) by JC-1

Detection of the mitochondrial membrane potential provides an early indication of cellular apoptosis. This process is typically defined as a collapse in the electrochemical gradient across the mitochondrial membrane, as measured by the change in the mitochondrial membrane potential [67,68,69,70]. JC-1 was incorporated into cells and healthy mitochondria, in which it aggregates and fluoresces red (590 nm). When the mitochondrial membrane

potential collapses in apoptotic cells, the reagent no longer accumulates inside the mitochondria, and instead, it assumes a monomeric form which fluoresces green [71,72,73].

A loss of mitochondrial membrane potential leads to the induction of apoptosis in AuNPI3Cstreated EAC cells (Fig. 15 & 16).The quantitative analysis of JC-1–stained cells revealed a significant decrease in the red (high $\Delta\psi_m$) to green (low $\Delta\psi_m$) ratio in AuNPI3Cs-treated cells compared with control cells.

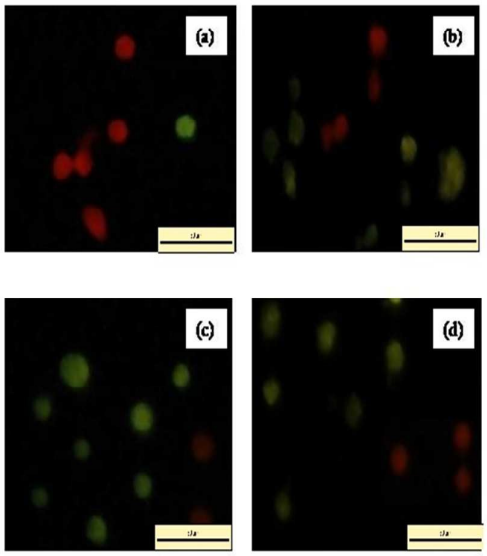

Fig. 15 JC-1 fluorescence imaging of mitochondria. Green fluorescence, depolarized (monomer) mitochondria; red fluorescence, hyperpolarized (J aggregates) mitochondria.(**a)** Control; (b) I3C-treated cells; (c) AuNPI3C-treated cells; (d) 5-FU-treated cells.

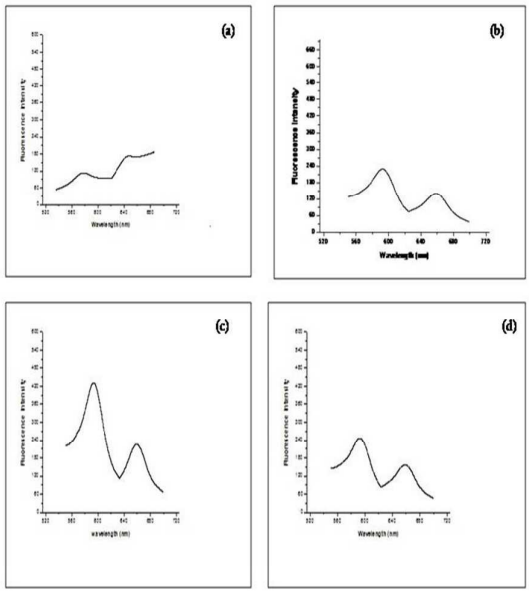

Fig. 16 Intensity of mitochondrial membrane potential in EAC cells analyzed by fluorescence spectrophotometer. The first peak represents the green fluorescence (Excitation 514 nm, Emission 529 nm) intensity and the last peak represents the red fluorescence (Excitation 585 nm, and Emission 590 nm) intensity. (**a)** Control; (b) I3C-treated cells; (c) AuNPI3C- treated cells; (d) 5-FU - treated cells.

Genotoxic effect by Alkaline Comet assay

EAC cells treated with AuNPI3Cs showed significant increase ($p<0.001$) in percentage of tail DNA intensity compared to EAC control. The fluorescence images (Fig. 17) are highly correlated with the percentage of tail DNA intensity level (Fig. 18). From our result, the comet assay confirmed the potent genotoxic effects of AuNPI3Cs on carcinoma cells. The

increase in the percentage of tail DNA intensity may be as a result of direct induction of DNA strand breakage by nanoparticles, such as free radicals. It had been found that many chemically synthesized nanoparticles cause genotoxic effects, such as oxidative DNA damage, point mutation and DNA strands break etc. Although the mechanism of nanoparticles-induced genotoxicity has not been clearly understood, early it had been found that nanoparticles are permeable to the nuclear membrane and then interact with DNA directly or indirectly[74].

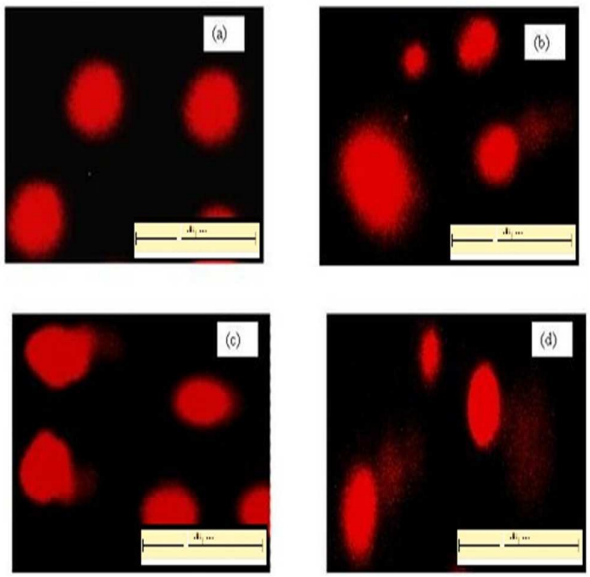

Fig. 17 Genotoxic effects of AuNPI3Cs in EAC cells by Comet assay. Fluorescent microscopic image of (a) EAC-Control; (b) I3C-treated EAC cell ; (c) AuNPI3Cs-treated EAC cell; and (d) 5-FU treated-EAC cell

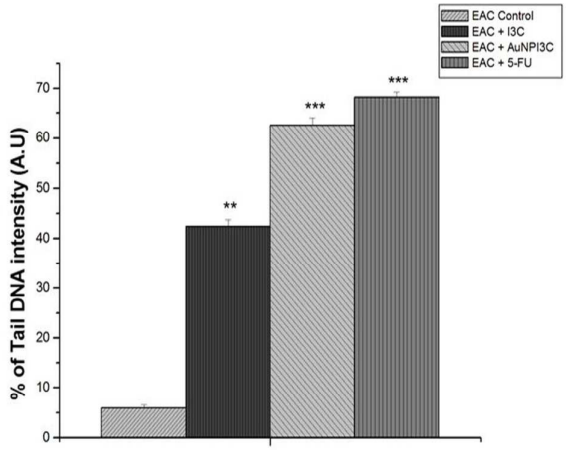

Fig. 18 Estimation of the percentage of tail DNA intensity of EAC cells treated with I3C, AuNPI3Cs and 5-FU. Values are expressed as the means ± SEM of three experiments; '***' indicate significant differences ($p<0.001$) compared with control group.

Cellular apoptosis by flow cytometry

Cell cycle deregulation is the most frequently observed phenomenon in cancer development. Several phytochemicals have been reported to inhibit the growth of cancer cells through cell cycle arrest[75]. From Fig. 20 it is clear that cell population is increased in G_2/M phase after AuNPI3Cs treatment. So, the present study indicates that AuNPI3Cs could induce G_2/M phase arrest (Fig. 19) in EAC cells. The G_2/M phase cell cycle arrest serves to prevent the cellfrom entering mitosis. Mitosis is regulated by Cdc2 and binding to cyclin B. This result suggests that DNA damage may extrude cyclin B1 from the nucleus, which promotes G_2/M phase arrest[76].

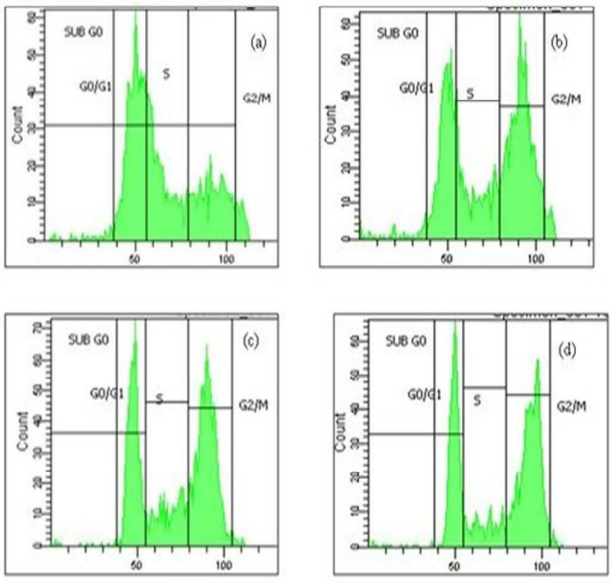

Fig. 19 cell cycle-based apoptosis assay. Cells were treated with respective IC50 of AuNPI3Cs for 24 hours, stained with PI and measured by flow cytometry. (a) EAC Control; (b) I3C-treated EAC cell ; (c) AuNPI3Cs-treated EAC cell; and (d) 5-FU-treated EAC cell.

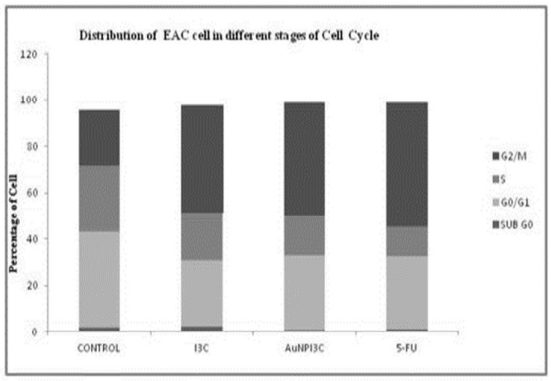

Fig. 20 The percentage of EAC cells in different phases of cell cycle from flow cytometric analysis. Accumulation of G_2/M cells plotted from the cell cycle-based apoptosis assay.

Conclusions

We have demonstrated that an eco-friendly and cost-effective protocol for synthesizing AuNPs using indole-3-carbinol at room temperature. It can be concluded that indole-3-carbinol is responsible for capping the AuNPs as confirmed from FTIR studies. AuNPI3Cs in 2-3 nm size range exhibited cytotoxicity on carcinoma cell in a dose-dependent manner, whereas it appeared to be less toxic in mice lymphocytes when exposed at doses up to 50 μg ml^{-1}. Furthermore, elevation of ROS and cell cycle arrest in G_2/M phase in AuNPI3Cs-

exposed EAC cells indicates the possible contribution of apoptosis in the aetiology of EAC cell death.

Based on these results, it is interpreted that oxidative stress and induction of apoptosis are the possible anticancer mechanisms in EAC cells by AuNPI3Cs. The application of AuNPI3Cs may lead to an invention of possible antiapoptotic agent in cancer therapy.

Acknowledgements

The author, Ananya Pradhan gratefully acknowledge to DST, Govt. of India, for providing fellowship under INSPIRE fellowship.

The authors are thankful to Vidyasagar University,Midnapore for providing the facilities to execute these studies. The authors would like to express their gratefulness to Indian Institute of Technology,Kharagpur, Indian Institute of Chemical Biology, Kolkata and Bose Institute, Kolkata for instrumental facilities.

Declaration of Interest

The Authors declare that there are no conflicts of interest.

Notes and References

1 M.I.Sriram, S.B.M.Kanth, K.Kalishwaralal and S.Gurunathan ,*International Journal of Nanomedicine*,2010, **5**, 753–762

2 S. K.Sahoo, F. Dilnawaz and S.Krishnakumar,*DrugDiscov Today*, 2008,**13**,144–151.

3 R. Raghavendra, K. Arunachalam, S. K.Annamalai and A. M. Arunachalam, *International Journal of Pharmacy andPharmaceuticalSciences.*, 2014, **6**, 74-87.

4 J. Siemieniec and P. Kruk, *CHEMIK.*,2013,**67**, 842-847.

5 W. Cai, T. Gao, H. Hong and J. Sun, *Nanotechnology, Science and Applications.*, 2008,**1**,17–32.

6 M. A. Hayat, *San Diego, CA: Academic Press*, 1989,1 and 2.

7 J. Turkevich and P. H. J. Stevenson, *Discuss. Faraday Soc*., 1951,**11**, 55-75.

8 X. Li, H. Xu, Z-S. Chen and G. Chen, *Journal of nanomaterials.*,2011, **2011**.

9S. Guo and E. Wang, *AnalyticaChimicaActa.*,2007,**598**, 181-192.

10 A. R. Sperling, R. P. Gil, F. Zhang, M. Zanella and J. W. Parak, *Chemical Society Reviews*, 2008,**37**, 1896-1908.

11 J. A. Ho, H. C. Chang, N. Y. Shih, L. C. Wu, Y. F. Chang, C. C. Chen and C. Chou, *Anal. Chem*., 2010, **82**, 5944–5950.

12 E. Boisselier and D. Astruc, *Chem. Rev*., 2009, **38**, 1759–1782.

13 J. L. Gardea-Torresdey, J. G. Parsons, E. Gomez, J. Peralta-Videa, H. E. Troiani, P. Santiago, and M. Jose Yacaman, *Nano Letters.*, 2002,**2**, 397-401.

14 A. D. Dwivedi and K. Gopal, *Colloids and Surfaces A: Physicochem. Eng. Aspects.*,2010,**369**, 27-33.

15 S. S. Shankar, A. Rai, A. Ahmad and M. Sastry, *Chem. Mater*., 2005, **17**, 566

16 A. Ahmad , S. Senapati , M. I. Khan , R. Kumar and M. Sastry, *Langmuir*,2003,**19**, 3550–3553.

17 H. Shiying , G. Zhirui, Y. Zhanga, S. Zhanga, J. Wanga and G. Ning, *Material Letters.*,2007,**61**, 3984–3987.

18 N. Law, S. Ansari ,F. R. Livens, J. C. Renshaw and J. R. Lloyd, *Appl. Environ. Microbiol*., 2008,**74**, 7090–7093.

19 N. Saifuddin, C. W. Wong and A. A. Nuryasumira, *E-Journal of Chemistry.*, 2009,**6**, 61–70.

20 H. Bao, Z. Lu, X. Cui, J. Guo, J. M. Anderson and C. M. Li, *Acta Biomater*.,2010, **6**, 3534–3541.

21 P. Ghosh,G. Han , M. De , C. K. Kim and V. M. Rotello, *Adv Drug Del Rev*., 2008, **60**,1307-15.

22 D. Raghunandan, S. Basavaraja, B. Mahesh, S. Balaji, S. Y. Manjunath, and A. Venkataraman, *Nanobiotechnol*.,2009,**5**,34–41

23 S. MaitiChoudhury, M. Gupta and U. K. Majumder, *Oxidative Medicine and Cellular Longevity.*, 2010, **3**, 61- 70

24 L. Hudson and F. C. Hay, *Blackwell Pub, Oxford, 3rd edn*, 1989.

25 S. K. Sahu, S. K. Mallick, S. Santra , T. K. Maiti, S. K. Ghosh and P. Pramanik,*J. Mater. Sci. Mater. Med.*,2010,**21**, 1587–1597.

26 P. Sanpui , A. Chattopadhyay , S. S. Ghosh . *ACS Appl Mater Interfaces*., 2011, **3**,218–228

27 D. Peer ,J. M. Karp , S. Hong ,O. C. Farokhzad,R. Margalit and R. Langer . *Nat Nanotechnol*., 2007,**2**,751

28 T. Ghosh,T. Chattopadhyay, S. Das , S. Mondal, E. Suresh ,E. Zangrando and D. Das, *Cryst Growth Des.*,2011,**11**,3198–3205.

29 E. Papis, F. Rossi , M. Raspanti, D. D. Isabella , G. Colombo , A. Milzani, G. Bernardini and R. Gornati ,*Toxicol Lett.*, 2009,**189**,253-259

30 A. Kumar, M. L. Garg, N. Singh and V. Vijayan, *Indian Journal of Pure & Applied Physics.,*2006,**44**,300-307.

31 T. Mosmann, *J. Immunol. Methods*.,1983,**65**,55–63.

32 O. W.Griffith,*Journal of Biological chemistry*.,1981,**256**,4900-4904.

33 O. W.Griffith, *Anal Biochem*.,1980,**106**,207–212.

34A. Roy, A. Ganguly, S. Bose Dasgupta, B. D. Benu , C. Pal , P. Jaisankar and H. K. Majumder, *Mol. Pharmacol.*,2008,**74**,1292–1307.

35 O. H. Lowry ,N. J. Rosebrough, A. L. Farr, and R. J. Randall, *J. Biol. Chem*., 1951, **193**,265.

36 R. Prasad and B. Koch,*Biomed Res Int.*, 2014,**753451**,11.

37 K. Ho, L. S. Yazan, N. Ismail and M. Ismail, *Cancer Epidemiol*., 2009, **33**, 155-60.

38 J. Gong, F. Traganos and Z.Darzynkiewicz ,*Anal Biochem*.,1994,**218**,314–319

39 R. Sgonc, G. Boeck, H. Dietrich, J. Gruber, H. Recheis and G. Wick, *Trends in Genetics.,*1994,**10**, 41–42..

40P.M'Bemba-Meka, N. Lemieux and S. K.Chakrabarti,*Sci. Total Environ*., 2006, **369**,21–34.

41M. Salido, J. L. Gonzalez and J. Vilches,*Molecular cancer Therapeutics*.,2007,**6**,1292–9

42 D. D. Alcântara, H. F. Ribeiro, P. C. Cardoso, T. M. Araújo, R. R. Burbano, A. C. Guimarães, A. S. Khayat and B. M. Oliveira, *J. Appl. Toxicol*.,2011, **33**,151–156.

43 M. S. Bentle,K. E. Reinicke, E. A. Bey , D. R. Spitz and D. A. Boothman, *J. Biol. Chem*., 2006, **281**,33684–33696.

44 R. Nunez ,*Curr. Issues Mol. Biol*., 2001, **3**, 67-70.

45 M. Wang ,Q. Zhang , W. Hao and Z. X. Sun , *Chem. Cent. J*., 2011,**5**,73.

46 L. M. Liz and M. Tailoring, *Langmuir.*,2006,**22**, 32.

47 Joint Committee on Powder Diffraction Standards, Diffraction Data File: JCPDS International Center for Diffraction Data. Swarthmore PA. 1991.

48 J. Schmitt and H. C. Flemming,*IntBiodeteriorBiodegrad.*,1998, **41**,1–11

49 C. W. Brown, Y. Li , J. A. Seelenbinder, P. Pivarnik, A. G. Rand , S. V. Letcher, O. J. Gregory and M. J. Platek, *Anal Chem*.,1998,**70**,2991–2996

50 J. A. Seelenbinder, C. W. Brown , P. Pivarnik and A. G. Rand,*Anal Chem*.,1999, **71**,1963–1966

51A. A. Kamnev, L. A. Dykman, P. A. Tarantilis and M. G. Polissiou.*Biosci Rep*.,2002,**22**,541–547

52 F. P. Gao, H. Z. Zhang, L. R. Liu, Y. S. Wang, Q. Jiang, X. D. Yang and Q. Q. Zhang, *Carbohydr. Polym.*, 2008, **71**,606.

53 S. P. Christopher ,*CancerMetstat Rev***.,**1992,**11**,179-195.

54 C. Grăvilă,S. Petrovici, L. Stana, L. Olariu and A. Trif, *J. Agroaliment. Proc. Technol*.,2010, **16**,313–316.

55 L. A. Sena and N. S. Chandel, *Mol Cell*.,2012,**48**,158–167.

56 D. V. Pereira, F. Petronilho, H. R. Pereira, F. Vuolo, F. Mina, J. C. Possato, M. F. Vitto, D. R. de Souza, L. da Silva, M. M. da Silva Paula, C. T. de Souza and F. Dal-Pizzol, *Invest. Ophthalmol.Visual Sci*., 2012, **53**, 8036.

57 M. Jeyaraj, M. Rajesh, R. Arun, D. Mubarak Ali, G. Sathishkumar, G. Sivanandhan, G. K. Dev,M. Manickavasagam, K. Premkumar, N. Thajuddin and A. Ganapathi, *Colloids Surf., B*, 2013, **102**, 708.

58 H. M. Shen and S. Pervaiz, *FASEB J*., 2006, **20**, 1589.

59 G.Häcker, *Cell Tissue Res.*, 2000, **301**,5-17.

60 C. D. Bortner and J. A. Cidlowski, *Biochem Pharmacol*.,1998,**56**,1549–1559.

61 S. Suman, A. Pandey, and S. Chandna,*Cytotechnology*.,2012,**64**,9–14.

62 S. K. Sohaebuddin, P. T. Thevenot, D. Baker, J. W. Eaton and L. Tang, *Part. Fibre Toxicol.,*2010,**7**,22.

63 Y. Gavrieli, Y. Sherman, and S. A. Ben-Sasson, *Journal of Cell Biology.*, 1992, **119**, 493–501.

64Z. Darzynkiewicz, D. Galkowski, and H. Zhao, *Methods.*, 2008,**44**, 250–254.

65 C. Adrie, M. Bachelet, M. Vayssier-Taussat, F. Russo-Marie, I.Bouchaert, M.Adib-Conquy, J. M. Cavaillon, M. R. Pinsky, J. F.Dhainaut and B. S.Polla,*Am. J. Respir. Crit. Care Med.,*2001,**164**,389–395.

66 M. H. Yang and K. M. Schaich, *FreeRadic. Biol. Med.,*1996,**20**,225–236.

67J. D. Robertson and S. Orrenius,*Crit Rev Toxicol.,* 2000,**30**,609–27.

68L. Bouchier-Hayes, L. Lartigue and D. Newmeyer, *JClin Invest.,* 2005,**115**,2640–7

69J. S. Armstrong, *Br J Pharmacol.,* 2006,**147**,239–48.

70J. S. Armstrong, *Bioessays.,* 2006,**28**,253–60.

71A. Mathur, Y. Hong, B. K. Kemp, A. Alvarez and J. D. Erusalimsky,*Cardiovasc Res.,* 2000,**46**,126–38.

72V. N. Dedov, G. C. Cox and B. D. Roufogalis,*Micron.,* 2001,**32**,653–60.

73 M. Castedo, K. Ferri, T. Roumier, D. Metivier, N. Zamzami and G.Kroemer, *JImmunol Methods.,* 2002,**265**,39–47.

74 N. Asare, C. Instanes, W. J. Sandberg, M. Refsnes, P. Schwarze, M. Kruszewski, G.Brunborg, *Toxicology.,*2012,**291**,65–72.

75 C. Chen and A. N. Kong ,*Travels pharmacoScience*.,2005,**26**,318-326.

76 K. Drews-Elger, M. C. Ortells, A. Rao, C. López-Rodriguez, J. Aramburu,*PLoS One.,* 2009, **4**,e5245.

Graphical Abstract